IEEE Access
Multidisciplinary : Rapid Review : Open Access Journal

Received October 14, 2020, accepted October 22, 2020, date of publication October 30, 2020, date of current version November 12, 2020.

Digital Object Identifier 10.1109/ACCESS.2020.3034917

Performance Analysis and Optimization for Power Beacon-Assisted Wireless Powered Cooperative NOMA Systems

YAFANG ZHANG, (Student Member, IEEE), SUILI FENG, (Member, IEEE), AND WEIJUN TANG, (Graduate Student Member, IEEE)

School of Electronic and Information Engineering, South China University of Technology, Guangzhou 510641, China

Corresponding author: Suili Feng (fengsl@scut.edu.cn)

ABSTRACT Wireless power transfer (WPT) is an effective way to prolong the lifetime of the energy-constraint networks. In this paper, we investigate a wireless powered cooperative non-orthogonal multiple access (WP-CNOMA) system, consisting of a power beacon (PB), an information transmitter (S), multiple relays (R) and two information receiving devices with near device D_1 and far device D_2. We assume both S and R are energy-constraint and there is no direct link between S and D_2. With the help of PB, S and R can harvest energy from it to restart the communication for WP-CNOMA network. For such a system, low-complexity but effective relay and antenna selection schemes are applied. To characterize the performance, outage probabilities and average throughput are derived for linear and non-linear energy harvesting (EH) models, respectively. Moreover, to maximize the average throughput, invoking the unimodal feature for average throughput with respect to the EH time, we find the optimal EH time via Golden section search method. Simulation results validate the accuracy of analytical results, and reveal the performance gain for our system over the benchmark schemes. Also, it can be seen that the non-linear EH model shows different outage behaviors from the linear one. On the other hand, considering the practical application and to improve the performance, the optimization for a simple WP-CNOMA system with single-antenna PB and single relay is also investigated, in which we aim to maximize the minimum throughput by jointly optimizing EH time and power allocation. A low-complexity analytical method is developed to find the max-min rate. Numerical results show that through optimization, the system performance can be improved significantly.

INDEX TERMS Antenna selection, non-orthogonal multiple access, non-linear energy harvesting, relay selection, wireless power transfer.

I. INTRODUCTION

Wireless power transfer (WPT) has emerged as a promising means to prolong the lifetime of the energy-constraint wireless networks, such as wireless sensor network (WSN) and mesh network in the field or post-disaster emergency communication [1]. There are two kinds of WPT-based network: one is simultaneous wireless information and power transfer (SWIPT) [2], in which radio frequency (RF) signals can carry information and energy simultaneously and then time switching (TS) or power splitting (PS) protocol is utilized at the receiver to harvest energy and decode signals separately; the other is wireless powered communication network (WPCN) [3], in which the energy-constraint nodes firstly harvest energy from the dedicated power station, such as power beacon (PB) or hybrid access point (HAP), and then use the harvested energy to perform the wireless information transfer (WIT). Both WPT models have been studied extensively in various scenarios. For SWIPT, the trade-off for rate and harvested energy for TS and PS protocols were investigated in [4] and [5], respectively. Moreover, performance analyses and optimization for its combination with cooperative relaying [6], cognitive radio [7], and distribution antenna systems [8] have also been studied deeply. For WPCN, the related works mainly include the applications into relaying network [9], [10], cognitive radio network [11], [12], cellular network [13] and unmanned aerial vehicle (UAV)-assisted communication [14].

The associate editor coordinating the review of this manuscript and approving it for publication was Tao Wang.

On the other hand, non-orthogonal multiple access (NOMA) is considered as a promising multiple access technique for 5G owing to its merits of massive connection, low delay and high spectral efficiency. Different from orthogonal multiple access (OMA), NOMA serves multiple users over the same time-frequency resource based on power-domain superposition coding (SC) at the transmitter and successive interference cancellation (SIC) at the receivers. It has been pointed out that NOMA has superior system throughput and fairness than OMA [15] and such performance gains can be enlarged by pairing users with distinct channel conditions [16]. However, even so, users with weaker channel conditions still have poor performance. In this case, invoking the merits of cooperative relaying for extending the coverage and improving reception performance, a lot of researchers turned their attention to the combination of cooperative relaying and NOMA (CNOMA). The first CNOMA scheme was proposed in [17], where relying on the prior information obtained from SIC, the cell-center user can act as a relay to help forward the information to the cell-edge user. Subsequently, a device-to-device (D2D)-aided cooperative NOMA scheme was proposed in [18]. In parallel, the CNOMA networks involved with dedicated relay have also been extensively discussed. In [19], a NOMA in coordinated direct and relay transmission scheme was introduced, where the BS communicated with cell-center user directly and communicated with the cell-edge user with the help of dedicated relay. Furthermore, a relay-assisted multi-user CNOMA system was proposed in [20]. It should be noted that the superiority of CNOMA over the corresponding OMA scheme has been demonstrated in the above-mentioned works. To seek further performance improvement, a lot of efforts have been made, such as low-complexity relay/antenna selection [21] and optimization [22], [23]. However, we can find that the above-mentioned works focused on the scenarios that all the nodes have stable power supply. But, in practical scenarios such as places suffered from the natural disaster, in the tunnel or in the field, the wireless devices may be energy-constraint, and replacing or recharging their batteries are high-cost or even impossible. How to complete the communication for such scenarios and improve their spectral efficiency simultaneously?

To this end, plenty of researchers put their efforts into the combination of WPT, NOMA and cooperative relaying. There are three main branches: the first line is pure NOMA and SWIPT. For such network, the PS or TS optimization combined with NOMA power allocation was a major consideration [24], [25]. The second line is CNOMA and SWIPT (SWIPT-CNOMA), in which the cell-center users or relay exploited TS, PS or hybrid TS-PS protocol to harvest energy from source and then helped forward information to the cell-edge users [26], [27]. Most researchers focused on its outage analysis [26]–[28] while the power allocation and TS/PS ratio optimization have also been investigated [29], [30]. The third line is NOMA and WPCN (WPCN-NOMA). Most existing works mainly focused on the optimization for such network to find the optimal energy harvesting (EH) time and power allocation [31]–[34]. The authors in [31] optimized the duration of WPT for an uplink multiuser WPCN-NOMA system. Both objectives for maximizing minimum rate and maximizing system throughput were considered. Following by [31], the common throughput maximization problem with the energy causality constraint was investigated in [32]. In [34], a transmit power minimization problem for a downlink wireless-powered multiple-input-single-output NOMA system was proposed.

Although excellent researches have been conducted on WPCN-NOMA, very few works have focused on the combination of cooperative NOMA and WPCN. Recently, the scenario for PB charging transmitter and relay has been widely adopted in existing works [9], [35], [36], but they mainly focused on the communication for three-node (source-relay-destination) model. However, the future communication systems are characterized by massive connectivity. Inspired by these observations, in this paper, we propose a wireless-powered cooperative NOMA (WP-CNOMA) system consisting of a power beacon B, an information transmitter S, multiple relays (R), and two information receiving devices (the near one denoted for D_1 and the far one denoted for D_2). In line with [12], [34] and [37], we assume S and R are energy-constraint, so they need to harvest energy from B. Note that, in such network, relay can not only assist the data transmission, but also alleviate the challenge for the low-efficiency of WPT. As a result, powered by B, S can communicate with D_2 with the aid of relays. The main differences for our system from the existing ones exist in the following aspects: First, for the B charging S and R model, the existing works mainly focused on the case in which only one receiver was involved [9], [35], [36], while we consider the communication of multiple receivers using NOMA. Second, most of the existing works used the linear EH model to study the performance of WPT-based system by assuming the harvested energy was linearly increased with the RF power [26]–[28]. However, in practical, the EH circuit shows non-linear behaviors due to the nonlinearity for the electronic devices [35]. In line with [35], [38], in this paper, the non-linear EH model is considered for the outage analysis of our WP-CNOMA system. Third, the optimization in [30] for single-input-single-output (SISO) SWIPT-CNOMA system is much different from the optimization of WPCN-CNOMA system since the rate expressions of the latter are more complex. Other existing works on WPCN-NOMA mainly obtained the solutions using high-complexity iterative algorithms [31], [34], in this paper, a low-complexity semi-analytical method is presented. In practice, the WP-CNOMA model may be adopted to cope with the energy-constraint challenge for WSN in the field or to achieve the temporary link re-establishing for emergency communication [13], [39]. The main contributions of this paper are summarized as follows:

- For the proposed WP-CNOMA system, two antenna selection (AS) schemes [9] as well as one partial relay selection scheme [36] are applied. To be specific, one

AS scheme selects the antenna that maximizes the harvested energy of S, which is called MES, while the other scheme selects the antenna that maximizes the harvested energy of R, which is called MER. For relay selection, the relay with the largest channel gain towards D_2 will be selected. Moreover, both linear and non-linear EH models are considered.

- We first derive the outage probabilities for two AS schemes under linear EH model and their average throughput are obtained. Moreover, the corresponding results under non-linear EH model are presented. Invoking the unimodal feature for average throughput with respect to (w.r.t.) EH time, the Golden section search method is exploited to find the optimal EH time.
- Considering the fact that the devices in WSN or in the Internet of Things (IoT) are usually characterized by low power and low cost [30], here a simple WP-CNOMA system with single-antenna PB and a single relay is considered. To improve the system performance, a minimum achievable rate maximization problem is developed by jointly optimizing the EH time and power allocation and a semi-closed-form optimal solution is obtained.
- Finally, simulation results are presented to validate the accuracy for our theoretical analyses and reveal the effects of the power of PB and the EH time on the performance of WP-CNOMA system and the performance gains over the benchmark schemes. Also, it can be found that the non-linear EH scheme shows different outage behavior from the linear one. In addition, by jointly optimizing power allocation and EH time, the performance of WP-CNOMA can be significantly improved.

The rest of this paper is organized as follows. In section II, we present the WP-CNOMA system model. In section III, we derive the outage probabilities and average throughput for linear and non-linear EH models, respectively. In section IV, optimization problem for maximizing the minimum throughput is considered. In Section V, we present the simulation results. Finally, section VI concludes this paper.

II. SYSTEM MODEL

We consider a WP-CNOMA system consisting of one power beacon B, one transmitter S, two receiving devices (the near one called D_1 and the far one called D_2), and K half-duplex (HD) relays R_j, $j \in \{1, 2, \cdots, K\}$, as shown in Fig.1. B is equipped with N antennas while all the other nodes are equipped with a single antenna. We assume there is no direct link between S and D_2 due to obstacles. It should be noted that the reason why we consider only two receivers is that the complexity of SIC for NOMA will increase with the number of multiplexed users. Also, the proposed model is typical and can be extended to multi-user scenarios with the help of user pairing, as reported in [22], [29]. In our model, S and relays are energy-constraint. In order to establish the communication connections between S and D_1 and D_2, B is introduced to charge S and relays. Usually, the energy harvested from WPT is limited and thus the coverage area is small, but the assistance of relay can effectively alleviate this problem. In this case, the communication for WP-CNOMA can be achieved.

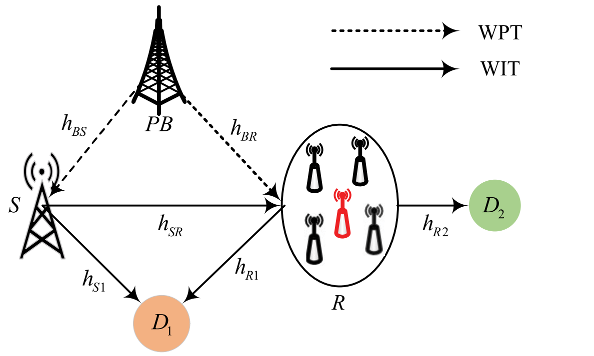

FIGURE 1. System model.

The channel coefficients for the links of the i-th antenna of B to S, the i-th antenna of B to R_j, S to D_1, S to R_j, R_j to D_1 and R_j to D_2 are assumed to be h_{B_iS}, $h_{B_iR_j}$, h_{S1}, h_{SR_j}, h_{R_j1}, h_{R_j2}, respectively, where $i \in \{1, 2, \cdots, N\}$ and $j \in \{1, 2, \cdots, K\}$. Without loss of generality, we assume that all the channels h_Ω, $\Omega \in \{B_iS, B_iR_j, S1, SR_j, R_j1, R_j2\}$ undergo the quasi-static independent and identically distributed (i.i.d.) Rayleigh fading. Therefore, the channel power gain $|h_\Omega|^2$ of link Ω follows exponential distribution with mean $E[|h_\Omega|^2] = d_\Omega^{-\alpha} = \lambda_\Omega$, where d_Ω is the inter-node distance for link Ω and α denotes the path loss exponent. As commonly assumed in works [21], [36], here we assume K relays are clustered relatively close together and thus there roughly has $\lambda_{R_j2} = \lambda_{R2}$. Similarly, we have $\lambda_{B_iS} = \lambda_{BS}$, $\lambda_{B_iR_j} = \lambda_{BR}$. In addition, we assume $d_{S1} < d_{SR} < d_{S2}$ [19], [23]. As a result, the probability density function (PDF) and cumulative distribution function (CDF) of $X = |h_\Omega|^2$ can be written as follows:

$$f_X(x) = \frac{1}{\lambda_\Omega} \exp(-\frac{x}{\lambda_\Omega}), \quad x > 0 \tag{1}$$

$$F_X(x) = 1 - \exp(-\frac{x}{\lambda_\Omega}), \quad x \geq 0 \tag{2}$$

Without loss of generality, we assume the power of the additive white Gaussian noise (AWGN) at all receivers is σ^2.

As shown in Fig. 2, the communication of WP-CNOMA system is comprised of two stages, namely EH phase and information transmission phase. Specifically, the first stage with duration of τT is spent for B to charge S and R and the remaining time of $(1-\tau)T$ is used for WIT. During the WIT stage, HD relay R will use separate time slots with

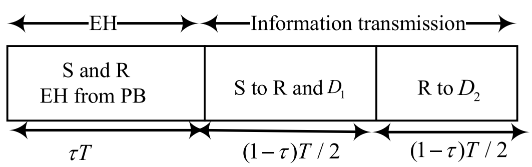

FIGURE 2. Protocols of WPT and WIT for WP-CNOMA system.

same duration $(1-\tau)T/2$ to complete the direct transmission from S to R and D_1 and the cooperative transmission from R to D_2, respectively. Note that here we assume two equal durations are allocated for direct transmission and cooperative transmission and this assumption is widely used in HD relay-assisted networks [9]–[12], [27], [29]. For simplicity, we consider a normalized time with $T = 1$.

Prior to transmission, relay and antenna selections are carried out. For relay selection, we choose the one that has the best channel towards D_2, that is, $R_c = \arg\max_{j=1,\cdots,K} \{|h_{R_j2}|^2\}$. Followed by relay selection, two commonly used AS schemes are presented for B to select the best antenna B_c. In scheme 1 (MES), B chooses the antenna that maximizes the harvested energy of S, so we have $B_c = \arg\max_{i=1,\cdots,N} \{|h_{B_iS}|^2\}$. While in scheme 2 (MER), B chooses the one that maximizes the harvested energy of R, which can be described as $B_c = \arg\max_{i=1,\cdots,N} \{|h_{B_iR_c}|^2\}$. It's noteworthy that as mentioned in [27], transmit AS is a low-complexity scheme for multi-antenna BS, which achieves a good tradeoff of the diversity gain and the implementation cost. While in WPT, beamforming at multi-antenna BS enables the energy-constraint nodes to harvest more energy. For the analysis of such system, we first need to find the optimal energy beamforming vector and then derive the PDF and CDF expressions of the effective channel gains involved with beamforming vector, which needs further in-depth study. Here we mainly focus on the performance for WP-CNOMA using AS. The following we look into the WPT and WIT stages for WP-CNOMA.

A. WPT STAGE

For the WPT stage, with the selected antenna and relay, B will broadcast the RF signal. As a result, the input power for the EH circuit will be $P_{\Delta}^{in} = |h_{B_c\Delta}|^2 P_B$, where $\Delta \in \{S, R_c\}$, and P_B is the transmit power of B. We assume P_B is significantly greater than the power of noise so the energy harvested from noise is ignored [36].

In this paper, both the linear and non-linear EH models are considered. For the linear EH model, the harvested energy for node Δ can be given by

$$E_{\Delta} = \eta\tau T|h_{B_c\Delta}|^2 P_B, \quad \Delta \in \{S, R_c\} \tag{3}$$

where η is the energy conversion efficiency. However, considering the non-linear characteristic for practical EH circuit, the corresponding harvested energy expressions can be given by [35]

$$E_{\Delta} = \begin{cases} \eta\tau T P_{\Delta}^{in}, & P_{\Delta}^{in} \leq P_{th}^{\Delta} \\ \eta\tau T P_{th}^{\Delta}, & P_{\Delta}^{in} \geq P_{th}^{\Delta} \end{cases} \tag{4}$$

where P_{th}^{s} and P_{th}^{r} characterize the maximum harvested power values at S and R, respectively, when their EH circuits are saturated. In view of the WIT protocol, the transmit powers at S and R can be expressed as

$$P_{\Delta} = \frac{E_{\Delta}}{(1-\tau)T/2} \tag{5}$$

In the sequel of this paper, we will use the superscripts L and NL to denote the linear and non-linear EH models, respectively. For L-MES scheme, the transmit powers at S and R can be respectively written as

$$P_S^{L-MES} = 2\xi P_B \cdot \max_{i=1,\cdots,N}(|h_{B_iS}|^2) \tag{6}$$

$$P_R^{L-MES} = 2\xi P_B |h_{B_cR_c}|^2 \tag{7}$$

where $\xi = \eta\tau/(1-\tau)$. While For L-MER scheme, the harvested powers at S and R can be respectively written as

$$P_S^{L-MER} = 2\xi P_B |h_{B_cS}|^2 \tag{8}$$

$$P_R^{L-MER} = 2\xi P_B \cdot \max_{i=1,\cdots,N}(|h_{B_iR_c}|^2) \tag{9}$$

In NL-MES and NL-MER schemes, we have

$$P_S^{NL-MES} = \begin{cases} P_S^{L-MES}, & P_S^{in} < P_{th}^{s} \\ 2\xi P_{th}^{s}, & P_S^{in} \geq P_{th}^{s} \end{cases} \tag{10}$$

$$P_R^{NL-MES} = \begin{cases} P_R^{L-MES}, & P_R^{in} < P_{th}^{r} \\ 2\xi P_{th}^{r}, & P_R^{in} \geq P_{th}^{r} \end{cases} \tag{11}$$

where $P_S^{in} = \max_{i=1,\cdots,N}(|h_{B_iS}|^2)P_B$ and $P_R^{in} = |h_{B_cR_c}|^2 P_B$. And

$$P_S^{NL-MER} = \begin{cases} P_S^{L-MER}, & P_S^{in} < P_{th}^{s} \\ 2\xi P_{th}^{s}, & P_S^{in} \geq P_{th}^{s} \end{cases} \tag{12}$$

$$P_R^{NL-MER} = \begin{cases} P_R^{L-MER}, & P_R^{in} < P_{th}^{r} \\ 2\xi P_{th}^{r}, & P_R^{in} \geq P_{th}^{r} \end{cases} \tag{13}$$

where $P_S^{in} = |h_{B_cS}|^2 P_B$ and $P_R^{in} = \max_{i=1,\cdots,N}(|h_{B_iR_c}|^2)P_B$. From (6)–(13), we can find that for different combinations of EH models and AS schemes, the transmit power expressions of S and R will be changed.

B. WIT STAGE

For the first half of the remaining time, according to NOMA protocol, S uses the harvested energy to broadcast the superimposed signal $x_S = \sqrt{\beta_1 P_S}x_1 + \sqrt{\beta_2 P_S}x_2$ to D_1 and D_2, where $x_i, i = 1, 2$ denotes the message for D_i with $E[|x_i|^2] = 1$, and $\beta_i, i = 1, 2$ is the power allocation coefficient for D_i satisfying $\beta_1 + \beta_2 = 1$ and $\beta_1 < \beta_2$. P_S is the transmit power of S. In this duration, the received signals at D_1 and R_c can be respectively given by

$$y_1 = h_{S1}(\sqrt{\beta_1 P_S}x_1 + \sqrt{\beta_2 P_S}x_2) + n_1 \tag{14}$$

$$y_R = h_{SR_c}(\sqrt{\beta_1 P_S}x_1 + \sqrt{\beta_2 P_S}x_2) + n_R \tag{15}$$

where n_1 and n_R are the AWGNs at D_1 and R, respectively. Invoking SIC, D_1 firstly decodes x_2 and subtracts it from the observation and then begins to decode its own signal. To this end, we can express the received signal-to-interference-plus-noise ratio (SINR) expressions for D_1 to decode x_2, for D_1 to decode x_1 and for R to decode x_2 as

$$\gamma_{D_1 \to x_2} = \frac{|h_{S1}|^2\beta_2 P_S}{|h_{S1}|^2\beta_1 P_S + \sigma^2} \tag{16}$$

$$\gamma_{D_1\to x_1} = \frac{|h_{S1}|^2\beta_1 P_S}{\sigma^2} \quad (17)$$

$$\gamma_{R\to x_2} = \frac{|h_{SR_c}|^2\beta_2 P_S}{|h_{SR_c}|^2\beta_1 P_S+\sigma^2} \quad (18)$$

respectively. Once successfully decoded, R will forward x_2 to D_2 with power P_R, so the received signal at D_2 can be given by

$$y_2 = h_{R_c2}\sqrt{P_R}x_2 + n_2 \quad (19)$$

where n_2 is the AWGN at D_2. As a result, the received SINR for D_2 to decode x_2 will be

$$\gamma_{D_2\to x_2} = \frac{|h_{R_c2}|^2 P_R}{\sigma^2} \quad (20)$$

Since the DF relaying protocol is exploited in our network, combined with (16), (17), (18) and (20), the achievable rates of D_1 and D_2 can be respectively formulated as follows:

$$R_1 = \frac{1-\tau}{2}\log_2\left(1+\gamma_{D_1\to x_1}\right) \quad (21)$$

$$R_2 = \frac{1-\tau}{2}\log_2(1+\min\{\gamma_{D_1\to x_2}, \gamma_{R\to x_2}, \gamma_{D_2\to x_2}\}) \quad (22)$$

III. OUTAGE PROBABILITY ANALYSIS

In this section, we will investigate the outage performance for our system. Outage probability (OP) denotes the probability that the achievable rate is smaller than the target data rate. In WPT-based system, the effective channel is usually the product of WPT channel and WIT channel when the transmitter is energy-constraint. In this case, the theoretical analyses become much complicated compared with the systems that are not involved with EH. To facilitate the subsequent OP analysis, the related CDFs of some special random variables such as $X = |h_{ij}|^2|h_{mn}|^2$ and $Z = |h_{mn}|^2 \cdot \max_{i=1,\cdots,N}|h_{Bij}|^2$ are presented in the following lemmas:

Lemma 1: The CDF of $X = |h_{ij}|^2|h_{mn}|^2$ can be given by

$$\begin{aligned} F_X(x) &= 1 - 2\sqrt{\frac{x}{\lambda_{ij}\lambda_{mn}}}K_1\left(2\sqrt{\frac{x}{\lambda_{ij}\lambda_{mn}}}\right) \\ &= 1 - W\left(\frac{4x}{\lambda_{ij}\lambda_{mn}}\right) \end{aligned} \quad (23)$$

where $K_v(\cdot)$ is the modified Bessel function of the second kind with order v [40, eq.(3.471.9)]. Here $W(x) = \sqrt{x}K_1(\sqrt{x})$ is introduced for notation simplification.

Proof: The CDF of X can be formulated as follows

$$\begin{aligned} F_X(x) &= \Pr(|h_{ij}|^2|h_{mn}|^2 < x) \\ &= \int_0^\infty f_{|h_{ij}|^2}(y)F_{|h_{mn}|^2}(x/y)dy \end{aligned} \quad (24)$$

Substituting (1) into (24), and invoking [40, eq.(3.324.1)], (23) can be obtained. ■

Assume $|h_{Bij}|^2 \sim CN(0,\lambda_{Bj}), i = 1,\cdots,N, j \in \{S, R_c\}$, that is to say, all the channels between each antenna of B and node j are independent and identically distributed. Therefore, the following lemmas can be obtained:

Lemma 2: The CDF and PDF of $V = \max_{i=1,\cdots,N}|h_{Bij}|^2$ can be provided as follows

$$F_V(v) = 1 - \sum_{i=1}^{N}\binom{N}{i}(-1)^{i-1}e^{-\frac{iv}{\lambda_{Bj}}} \quad (25)$$

$$f_V(v) = \sum_{i=1}^{N}\binom{N}{i}\frac{i(-1)^{i-1}}{\lambda_{Bj}}e^{-\frac{iv}{\lambda_{Bj}}} \quad (26)$$

Proof: The CDF of V can be formulated as follows:

$$\begin{aligned} F_V(v) &= \Pr(\max_{i=1,\cdots,N}|h_{Bij}|^2 < z) \\ &\overset{(a)}{=} \left[1-\exp(-v/\lambda_{Bj})\right]^N \\ &\overset{(b)}{=} 1 - \sum_{i=1}^{N}\binom{N}{i}(-1)^{i-1}e^{-\frac{iv}{\lambda_{Bj}}} \end{aligned} \quad (27)$$

where (a) is conditioned on the assumption that the channels between each antenna of B and node j are independent and experience the identical exponential distribution with parameter λ_{Bj}. (b) follows from the Binomial Theorem and $\binom{N}{i} = \frac{N!}{i!(N-i)!}$. As a result, taking the derivation for $F_V(v)$ w.r.t. v, the PDF of V can be obtained. ■

Lemma 3: The CDF of $Z = |h_{mn}|^2 \cdot \max_{i=1,\cdots,N}|h_{Bij}|^2$ can be given by

$$F_Z(z) = 1 - \sum_{i=1}^{N}\binom{N}{i}(-1)^{i-1}W\left(\frac{4iz}{\lambda_{Bj}\lambda_{mn}}\right). \quad (28)$$

Proof: Let $X = |h_{mn}|^2$ and $V = \max_{i=1,\cdots,N}|h_{Bij}|^2$, we can formulate the CDF of Z as

$$F_Z(z) = \int_0^\infty f_X(x)F_V(z/x)dx \quad (29)$$

Substituting (25) into (29) and invoking [40, eq.(3.324.1)], the CDF of Z can be obtained. ■

A. OP ANALYSIS FOR LINEAR EH SCHEME

Let $R_{1,th}$ and $R_{2,th}$ denote the target data rates to decode x_1 and x_2, respectively. Considering the cooperative NOMA protocol, the outage event at D_1 will occur when D_1 cannot successfully decode x_2 or when D_1 enables to decode x_2, but it cannot decode its own signal. That is to say, when both x_1 and x_2 can be successfully decoded at D_1, the outage of D_1 will not occur. As a result, the OP of D_1 can be formulated as

$$P_{out,1} = 1 - \Pr(\gamma_{D_1\to x_2} \geq \omega_2, \ \gamma_{D_1\to x_1} \geq \omega_1) \quad (30)$$

where $\omega_i = 2^{2R_{i,th}/(1-\tau)} - 1, i = 1, 2$ represents the SINR threshold for decoding x_i. While the outage event of D_2 occurs when R or D_2 cannot decode x_2, so the OP of D_2 can be expressed as

$$P_{out,2} = 1 - \Pr(\gamma_{R\to x_2} \geq \omega_2, \ \gamma_{D_2\to x_2} \geq \omega_2) \quad (31)$$

In the following, we will explore the outage performance for the WP-CNOMA system with L-MES, L-MER, NL-MES and NL-MER schemes, respectively. For convenience of presentation, in what follows, we use X_i, Y_i, and Z_j to represent $\max\limits_{i=1,\cdots,N}|h_{B_iS}|^2$, $\max\limits_{i=1,\cdots,N}|h_{B_iR}|^2$ and $\max\limits_{j=1,\cdots,K}|h_{R_j2}|^2$, respectively.

1) OP WITH L-MES

Substituting (6), (16) and (17) into (30), the OP of D_1 with L-MES can be rewritten as

$$\begin{aligned}P_{out,1}^{L-MES} &= 1-\Pr\left(\frac{\beta_2|h_{S1}|^2X_i}{\beta_1|h_{S1}|^2X_i+1/(2\xi\rho)}\geq\omega_2,\right.\\ &\left.\quad 2\xi\rho\beta_1|h_{S1}|^2X_i\geq\omega_1\right)\\ &=\Pr\left(|h_{S1}|^2X_i<u/(2\xi\rho)\right)\end{aligned}\tag{32}$$

where $\rho = P_B/\sigma^2$ denotes the transmit signal-to-noise ratio (SNR) of B, and $u=\max\{\theta_1,\theta_2\}$ with $\theta_1=\omega_1/\beta_1$ and $\theta_2=\omega_2/(\beta_2-\omega_2\beta_1)$. Note that (32) holds in the condition of $0<\omega_2<\beta_2/\beta_1$, otherwise, there will be $P_{out,1}^{L-MES}=1$. With the aid of Lemma 3, $P_{out,1}^{L-MES}$ can be obtained as

$$P_{out,1}^{L-MES}=1-\sum_{i=1}^{N}\binom{N}{i}(-1)^{i-1}W\left(\frac{2iu}{\lambda_{BS}\lambda_{S1}\xi\rho}\right)\tag{33}$$

While for D_2, substituting (6), (7), (18) and (20) into (31), the OP with L-MES will be

$$\begin{aligned}P_{out,2}^{L-MES} &= 1-\Pr\left(\frac{\beta_2|h_{SR_c}|^2X_i}{\beta_1|h_{SR_c}|^2X_i+1/(2\xi\rho)}\geq\omega_2,\right.\\ &\left.\qquad 2\,\xi\rho|h_{B_cR_c}|^2Z_j\geq\omega_2\right)\end{aligned}\tag{34}$$

Considering the independence for $S-R$ and $R-D_2$ links, we have

$$P_{out,2}^{L-MES}=1-I_1\cdot I_2\tag{35}$$

where

$$\begin{aligned}I_1 &= \Pr\left(|h_{SR_c}|^2X_i\geq\frac{\theta_2}{2\xi\rho}\right)\\ &=\sum_{i=1}^{N}\binom{N}{i}(-1)^{i-1}W\left(\frac{2i\theta_2}{\lambda_{BS}\lambda_{SR}\xi\rho}\right)\end{aligned}\tag{36}$$

where (36) holds conditioned on $0<\omega_2<\beta_2/\beta_1$, otherwise, $I_1=0$. With the aid of Lemma 3, we can derive I_2 as follows

$$\begin{aligned}I_2 &= \Pr\left(|h_{B_cR}|^2Z_j\geq\frac{\theta_2}{2\xi\rho}\right)\\ &=\sum_{j=1}^{K}\binom{N}{j}(-1)^{j-1}W\left(\frac{2j\theta_2}{\lambda_{BR}\lambda_{R2}\xi\rho}\right)\end{aligned}\tag{37}$$

Combining I_1 and I_2, we can obtain

$$\begin{aligned}P_{out,2}^{L-MES} &= 1-\left[\sum_{i=1}^{N}\binom{N}{i}(-1)^{i-1}W\left(\frac{2i\theta_2}{\lambda_{BS}\lambda_{SR}\xi\rho}\right)\right]\\ &\quad\times\left[\sum_{j=1}^{K}\binom{N}{j}(-1)^{j-1}W\left(\frac{2j\theta_2}{\lambda_{BR}\lambda_{R2}\xi\rho}\right)\right]\end{aligned}\tag{38}$$

With (33) and (38), the average system throughput with L-MES scheme can be given by [26]

$$C^{L-MES}=(1-P_{out,1}^{L-MES})R_{th,1}+(1-P_{out,2}^{L-MES})R_{th,2}\tag{39}$$

2) OP WITH L-MER

With (8), (9), (16), (17), (18) and (20), the OPs of D_1 and D_2 using L-MER scheme can be presented by following theorems:

Theorem 1: The OP of D_1 in L-MER scheme can be given by

$$P_{out,1}^{L-MER}=1-W\left(\frac{2u}{\lambda_{BS}\lambda_{S1}\xi\rho}\right).\tag{40}$$

which holds in the condition of $0<\omega_2<\beta_2/\beta_1$, otherwise, there will be $P_{out,1}^{L-MER}=1$. Note that (40) can be easily obtained with the aid of Lemma 1, and thus it's proof is omitted.

Theorem 2: The OP of D_2 in L-MER scheme can be given by

$$\begin{aligned}&P_{out,2}^{L-MER}\\ &\quad=1-W\left(\frac{2\theta_2}{\lambda_{BS}\lambda_{SR}\xi\rho}\right)\\ &\qquad\times\left[\sum_{i=1}^{N}\sum_{j=1}^{K}\binom{N}{i}\binom{K}{j}(-1)^{i+j}W\left(\frac{2ij\omega_2}{\lambda_{BR}\lambda_{R2}\xi\rho}\right)\right]\end{aligned}\tag{41}$$

which holds in the condition of $0<\omega_2<\beta_2/\beta_1$, otherwise, there will be $P_{out,2}^{L-MER}=1$.

Proof: Similarly, substituting (8), (9), (18) and (20) into (31), and combining channel independence for $S-R$ and $R-D_2$ links, the OP of D_2 with L-MER can be rewritten as

$$P_{out,2}^{L-MER}=1-J_1\cdot J_2.\tag{42}$$

where J_1 can be calculated as follows

$$\begin{aligned}J_1 &= \Pr\left(\frac{\beta_2|h_{SR_c}|^2|h_{B_cS}|^2}{\beta_1|h_{SR_c}|^2|h_{B_cS}|^2+1/(2\xi\rho)}\geq\omega_2\right)\\ &=W\left(\frac{2\theta_2}{\lambda_{BS}\lambda_{SR}\xi\rho}\right)\end{aligned}\tag{43}$$

which follows from the condition of $0<\omega_2<\beta_2/\beta_1$, otherwise, $J_1=0$. Its detail derivation can refer to L-MES. Here we mainly focus on the derivation of J_2, which is presented as follows

$$\begin{aligned}J_2 &= \Pr\left(Y_iZ_j\geq\frac{\omega_2}{2\xi\rho}\right)\\ &=\int_0^{\infty}f_{Z_j}(z)\left[1-F_{Y_i}\left(\frac{\omega_2}{2\xi\rho z}\right)\right]dz\end{aligned}\tag{44}$$

Invoking Lemma 2 and based on [40, eq.(3.471.9)], we have

$$J_2=\sum_{i=1}^{N}\sum_{j=1}^{K}\binom{N}{i}\binom{K}{j}(-1)^{i+j}W\left(\frac{2ij\omega_2}{\lambda_{BR}\lambda_{R2}\xi\rho}\right)\tag{45}$$

Substituting J_1 and J_2 into (42), $P_{out,2}^{L-MER}$ can be obtained. ■

With (40) and (41), the average throughput with L-MER scheme can be written as

$$C^{L-MER} = (1 - P_{out,1}^{L-MER})R_{th,1} + (1 - P_{out,2}^{L-MER})R_{th,2} \quad (46)$$

B. OP ANALYSIS FOR NON-LINEAR EH SCHEME

By comparing (6)-(9) and (10)-(13), we can find that the non-linear EH model is different from the linear one. The main difference lies in that when the input power of the EH circuit is larger than the preset threshold, the non-linear EH model will tend to be saturated and thus the harvested energy will remain at a constant value. Therefore, it's necessary to further study the performance for WP-CNOMA system exploiting the non-linear EH model.

For the non-linear EH model, according to the EH states for S and R, following four cases need to be explored: (S_l, R_l), (S_l, R_∞), (S_∞, R_l) and (S_∞, R_∞), where S_l and R_l denote that S and R work in linear EH state, respectively, and S_∞ and R_∞ denote that S and R work in saturated EH state, respectively. For the sake of simplicity, we define C_{12} and C_1 as the events that D_1 can successfully decode x_2 and decode its own signal, respectively, and denote E_1 and E_2 as the events that R and D_2 can successfully decode x_2, respectively. As a result, the OPs of D_1 and D_2 under non-linear EH model can be respectively formulated as

$$P_{out,1} = 1 - [\underbrace{\Pr(S_l, C_{12}, C_1)}_{I_{11}} + \underbrace{\Pr(S_\infty, C_{12}, C_1)}_{I_{12}}] \quad (47)$$

Note that $P_{out,2}$, is shown at the bottom of this page. In (48), (a) follows from the channel independence for the direct link and cooperative link. (b) is to simplify the calculation. In addition, we can find that the OP of D_1 is simpler than that of D_2, since the OP of D_1 is independent of R while the OP of D_2 is affected by S and R.

1) OP WITH NL-MES

Invoking (10), (11), (16), (17), (18) and (20), the OPs of D_1 and D_2 with NL-MES can be provided as follows:

Theorem 3: The OP of D_1 in NL-MES scheme can be given by

$$P_{out,1}^{NL-MES} \approx 1 - (I_{11} + I_{12}). \quad (49)$$

which holds in the condition of $0 < \omega_2 < \beta_2/\beta_1$, otherwise, there will be $P_{out,1}^{NL-MES} = 1$ and I_{11} and I_{12} can be found in (51) and (52), respectively.

Proof: First, we start from the calculation of I_{11} in (47):

$$\begin{aligned} I_{11} &= \Pr(S_l, C_{12}, C_1) \\ &= \Pr\left(X_i P_B \le P_{th}^s, \frac{\beta_2 X_i |h_{S1}|^2}{\beta_1 X_i |h_{S1}|^2 + 1/(2\xi\rho)} \ge \omega_2, \right. \\ &\quad \left. 2\xi\rho\beta_1 X_i |h_{S1}|^2 \ge \omega_1\right) \\ &= \Pr\left(X_i \le \frac{P_{th}^s}{P_B}, X_i |h_{S1}|^2 \ge \frac{u}{2\xi\rho}\right) \\ &= \sum_{i=1}^{N} \binom{N}{i} \frac{i(-1)^{i-1}}{\lambda_{BS}} \int_0^{\frac{P_{th}^s}{P_B}} g(x)dx \end{aligned} \quad (50)$$

where $g(x) = \exp\left(-\frac{ix}{\lambda_{BS}} - \frac{u}{2\xi\lambda_{S1}\rho x}\right)$. As we all known, the closed-form expression of (50) is mathematically intractable. Here we exploit the Gaussian-Chebyshev quadrature [26] to approximate I_{11} as

$$I_{11} \approx \sum_{i=1}^{N} \binom{N}{i} \frac{i(-1)^{i-1}}{\lambda_{BS}} \sum_{l=1}^{L} \frac{\pi P_{th}^s \sqrt{1-y_l^2}}{2LP_B} g(x_l). \quad (51)$$

where $y_l = \cos(\frac{2l-1}{2L}\pi)$, $x_l = \frac{P_{th}^s}{2P_B}(y_l + 1)$, and L is a complexity-accuracy tradeoff parameter. Similarly, I_{12} can be calculated as follows:

$$\begin{aligned} I_{12} &= \Pr(S_\infty, C_{12}, C_1) \\ &= \Pr\left(X_i P_B \ge P_{th}^s, \frac{\beta_2 |h_{S1}|^2}{\beta_1 |h_{S1}|^2 + \sigma^2/(2\xi P_{th}^s)} \ge \omega_2, \right. \\ &\quad \left. 2\xi\beta_1 P_{th}^s |h_{S1}|^2 \ge \omega_1\right) \\ &= \sum_{i=1}^{N} \binom{N}{i} (-1)^{i-1} e^{-\frac{iP_{th}^s}{\lambda_{BS}P_B} - \frac{u\sigma^2}{2\xi\lambda_{S1}P_{th}^s}} \end{aligned} \quad (52)$$

Note that both results of I_{11} and I_{12} are conditioned on $0 < \omega_2 < \beta_2/\beta_1$, otherwise, $I_{11} = I_{12} = 0$. Substituting I_{11} and I_{12} into (47), the OP of D_1 with NL-MES can be obtained. ■

Similarly, the OP of D_2 can be given by the following theorem:

Theorem 4: The OP of D_2 in NL-MES scheme can be given by

$$\begin{aligned} P_{out,2}^{NL-MES} &\approx 1 - [\Pr(S_l, E_1) + \Pr(S_\infty, E_1)] \\ &\quad \times [\Pr(R_l, E_2) + \Pr(R_\infty, E_2)]. \end{aligned} \quad (53)$$

which holds in the condition of $0 < \omega_2 < \beta_2/\beta_1$, otherwise, there will be $P_{out,2}^{NL-MES} = 1$ and $\Pr(S_l, E_1)$, $\Pr(S_\infty, E_1)$, $\Pr(R_l, E_2)$ and $\Pr(R_\infty, E_2)$ can be found in (55), (56), (57) and (58), respectively.

$$\begin{aligned} P_{out,2} &= 1 - [\Pr(S_l, R_l, E_1, E_2) + \Pr(S_l, R_\infty, E_1, E_2) + \Pr(S_\infty, R_1, E_1, E_2) + \Pr(S_\infty, R_\infty, E_1, E_2)] \\ &\overset{(a)}{=} 1 - [\Pr(S_l, E_1)\Pr(R_l, E_2) + \Pr(S_l, E_1)\Pr(R_\infty, E_2) + \Pr(S_\infty, E_1)\Pr(R_l, E_2) + \Pr(S_\infty, E_1)\Pr(R_\infty, E_2)] \\ &\overset{(b)}{=} 1 - [\Pr(S_l, E_1) + \Pr(S_\infty, E_1)] \times [\Pr(R_l, E_2) + \Pr(R_\infty, E_2)] \end{aligned} \quad (48)$$

Proof: Similar to the derivation of $P_{out,1}^{NL-MES}$, here we first calculate $\Pr(S_l, E_1)$.

$$\begin{aligned}\Pr(S_l, E_1) &= \Pr\left(X_i P_B \le P_{th}^s,\ \frac{\beta_2 X_i |h_{SR_c}|^2}{\beta_1 X_i |h_{SR_c}|^2 + \sigma^2/(2\xi P_B)} \ge \omega_2\right) \\ &= \Pr\left(X_i \le \frac{P_{th}^s}{P_B},\ X_i |h_{SR_c}|^2 \ge \frac{\theta_2 \sigma^2}{2\xi P_B}\right) \end{aligned} \tag{54}$$

Applying the Gaussian-Chebyshev quadrature and invoking Lemma 3, we can obtain

$$\Pr(S_l, E_1) \approx \sum_{i=1}^{N} \binom{N}{i} \frac{i(-1)^{i-1}}{\lambda_{BS}} \sum_{l=1}^{L} \frac{\pi P_{th}^s \sqrt{1-y_l^2}}{2LP_B} H_1(x_l) \tag{55}$$

where $H_1(x) = \exp\left(-\frac{ix}{\lambda_{BS}} - \frac{\theta_2\sigma^2}{2\xi P_B \lambda_{SR} x}\right)$. As for the second term $\Pr(S_\infty, E_1)$, it can be derived as:

$$\begin{aligned}\Pr(S_\infty, E_1) &= \Pr\left(X_i P_B \ge P_{th}^s,\ \frac{\beta_2 |h_{SR_c}|^2}{\beta_1 |h_{SR_c}|^2 + \sigma^2/(2\xi P_{th}^s)} \ge \omega_2\right) \\ &= \Pr\left(X_i \ge \frac{P_{th}^s}{P_B}\right) \Pr\left(|h_{SR_c}|^2 \ge \frac{\theta_2\sigma^2}{2\xi P_{th}^s}\right) \\ &= \sum_{i=1}^{N} \binom{N}{i} (-1)^{i-1} e^{-\frac{iP_{th}^s}{\lambda_{BS} P_B} - \frac{\theta_2 \sigma^2}{2\xi \lambda_{SR} P_{th}^s}} \end{aligned} \tag{56}$$

Following the same methods, we have

$$\begin{aligned}\Pr(R_l, E_2) &= \Pr\left(|h_{B_cR_c}|^2 P_B \le P_{th}^r,\ 2\xi P_B |h_{B_cR_c}|^2 Y_j \ge \omega_2 \sigma^2\right) \\ &\approx \sum_{j=1}^{K} \binom{K}{j} \frac{(-1)^{j-1}}{\lambda_{BR}} \sum_{l=1}^{L} \frac{\pi P_{th}^r \sqrt{1-y_l^2}}{2LP_B} H_2(x_l^r) \end{aligned} \tag{57}$$

and

$$\begin{aligned}\Pr(R_\infty, E_2) &= \Pr\left(|h_{B_cR_c}|^2 P_B \ge P_{th}^r,\ 2\xi P_{th}^r Y_j \ge \omega_2 \sigma^2\right) \\ &= \sum_{j=1}^{K} \binom{K}{j} (-1)^{j-1} e^{-\frac{j\omega_2\sigma^2}{2\xi P_{th}^r} - \frac{P_{th}^r}{\lambda_{BR} P_B}} \end{aligned} \tag{58}$$

where $H_2(x) = e^{-\frac{x}{\lambda_{BR}} - \frac{j\omega_2\sigma^2}{2\xi\lambda_{R2} P_B x}}$ and $x_l^r = \frac{P_{th}^r(1+y_l)}{2P_B}$. Combining these four expressions, the OP of D_2 with NL-MES can be obtained. ■

To this end, the average throughput of WP-CNOMA with NL-MES can be given by

$$\begin{aligned} C^{NL-MES} &= (1-P_{out,1}^{NL-MES}) R_{th,1} + (1-P_{out,2}^{NL-MES}) R_{th,2} \end{aligned} \tag{59}$$

2) OP WITH NL-MER

Since the OP derivations for NL-MER are similar to NL-MES, the results will be directly presented by following theorems:

Theorem 5: The OP of D_1 in NL-MER scheme can be given by

$$P_{out,1}^{NL-MER} \approx 1 - (I_{11} + I_{12}). \tag{60}$$

where $I_{11} = \sum_{l=1}^{L} \frac{\pi P_{th}^s \sqrt{1-y_l^2}}{2L\lambda_{BS} P_B} T_1(x_l)$, $I_{12} = T_1\left(\frac{P_{th}^s}{P_B}\right)$ with $T_1(x) = e^{-\frac{x}{\lambda_{BS}} - \frac{u\sigma^2}{2\xi\lambda_{S1} P_B x}}$. Also, (60) is obtained in the condition of $0 < \omega_2 < \beta_2/\beta_1$, otherwise, $P_{out,1}^{NL-MER} = 1$.

Theorem 6: The OP of D_2 in NL-MER scheme can be given by

$$\begin{aligned} P_{out,2}^{NL-MER} \approx 1 &- [\Pr(S_l, E_1) + \Pr(S_\infty, E_1)] \\ &\times [\Pr(R_l, E_2) + \Pr(R_\infty, E_2)] \end{aligned} \tag{61}$$

where

$$\begin{aligned} \Pr(S_l, E_1) &\approx \sum_{l=1}^{L} \frac{\pi P_{th}^s \sqrt{1-y_l^2}}{2L\lambda_{BS} P_B} T_2(x_l) \\ \Pr(S_\infty, E_1) &= T_2\left(\frac{P_{th}^s}{P_B}\right) \\ \Pr(R_l, E_2) &= \sum_{i=1}^{N} \sum_{j=1}^{K} \binom{N}{i} \binom{K}{j} \frac{i(-1)^{i+j}}{\lambda_{BR}} \\ &\quad \times \sum_{l=1}^{L} \frac{\pi P_{th}^r \sqrt{1-y_l^2}}{2LP_B} T_3(x_l^r) \\ \Pr(R_\infty, E_2) &= \sum_{i=1}^{N} \sum_{j=1}^{K} \binom{N}{i} \binom{K}{j} (-1)^{i+j} T_3\left(\frac{P_{th}^r}{P_B}\right) \end{aligned}$$

with $T_2(x) = e^{-\frac{x}{\lambda_{BS}} - \frac{\theta_2\sigma^2}{2\xi\lambda_{SR} P_B x}}$ and $T_3 = e^{-\frac{ix}{\lambda_{BR}} - \frac{j\omega_2\sigma^2}{2\xi\lambda_{R2} P_B x}}$. Also, (61) holds conditioned on $0 < \omega_2 < \beta_2/\beta_1$, otherwise, $P_{out,2}^{NL-MER} = 1$.

As a result, the average throughput of WP-CNOMA with NL-MER can be given by

$$\begin{aligned} C^{NL-MER} &= (1 - P_{out,1}^{NL-MER}) R_{th,1} + (1 - P_{out,2}^{NL-MER}) R_{th,2} \end{aligned} \tag{62}$$

To effectively improve the system performance, here we consider an average throughput optimization problem with fixed power allocation (since the average throughput expression is much complicated, it's difficult to achieve joint time and power optimization), which is formulated as

$$\tau^* = \arg \max_{0 \le \tau < 1} \{C^M\} \tag{63}$$

where $M \in \{L-MES, L-MER\}$. Since the average throughput expressions are too complicated, some useful information such as monotonicity or concavity is hard to obtain from them. From the previous analytical results, it can be seen that the average throughput is closely related to the EH time.

Intuitively, when the EH time is small, the harvested energy is also small. In this case, it's likely that system will suffer outage; with the increase of EH time, this situation will gradually get better; if the EH time continues to increase, the time left for WIT will be less, so the outage probability will increase. Therefore, there exists an optimal EH time to maximize the average throughput. From the later simulation of the average throughput versus EH time, it can also be observed that the average throughput is an unimodal function w.r.t. τ. Therefore, we use the Golden section search (GSS) method [41] to find the optimal EH time.

IV. PERFORMANCE OPTIMIZATION

From the previous analyses, it can be seen that the EH time and power allocation have a significant impact on the performance of D_1 and D_2, but the joint time and power allocation optimization is difficult to realize from the perspective of average throughput. To obtain better performance, here we assume the perfect channel state information (CSI) is known and aim to maximize the achievable throughput. As mentioned in [30], the devices in WSN or in the IoT are characterized by low power and low cost, and thus here we focus on the optimal design for a simple WP-CNOMA system with $K = 1$ and $N = 1$, where $|h_{SR}|^2 < |h_{S1}|^2$. In this section, we aim to maximize the throughput under max-min rate criteria [42] by jointly optimizing the EH time τ and power allocation β, where β denotes the power proportion allocated to D_1. Based on (21) and (22), the optimization problem can be formulated as:

$$\max_{\tau,\beta} \ \min\{R_1, R_2\} \tag{64a}$$

$$\text{s.t. } 0 \le \tau < 1, 0 \le \beta < 1 \tag{64b}$$

$$R_1 = \frac{1-\tau}{2}\log_2\left(1+\frac{X\beta\tau}{1-\tau}\right) \tag{64c}$$

$$R_2 = \frac{1-\tau}{2}\log_2(1+\min\{\frac{Y(1-\beta)\tau}{(Y\beta-1)\tau+1}, \frac{Z\tau}{1-\tau}\}) \tag{64d}$$

where $X = \frac{\eta|h_{BS}|^2|h_{S1}|^2 P_B}{\sigma^2}$, $Y = \frac{\eta|h_{BS}|^2|h_{SR}|^2 P_B}{\sigma^2}$ and $Z = \frac{\eta|h_{BR}|^2|h_{R2}|^2 P_B}{\sigma^2}$. As discussed in [42], the problem of (64) can be rewritten as

$$(\tau^*, \beta^*) = \arg\max_{0\le\tau,\beta<1} \min\{I_1, I_2, I_3\} \tag{65}$$

where $I_1 = \frac{1-\tau}{2}\log_2(1+\frac{X\beta\tau}{1-\tau})$, $I_2 = \frac{1-\tau}{2}\log_2(1+\frac{Z\tau}{1-\tau})$ and $I_3 = \frac{1-\tau}{2}\log_2(1+\frac{Y(1-\beta)\tau}{(Y\beta-1)\tau+1})$. By observing the form of problem (65), we decompose it as following four subproblems:

$$(\text{Q1}): \max_{0\le\tau,\beta<1} I_2\,|_{\text{Case 1}} \tag{66}$$

$$(\text{Q2}): \max_{0\le\tau,\beta<1} I_3\,|_{\text{Case 2}} \tag{67}$$

$$(\text{Q3}): \max_{0\le\tau,\beta<1} I_1\,|_{\text{Case 3}} \tag{68}$$

$$(\text{Q4}): \max_{0\le\tau,\beta<1} I_3\,|_{\text{Case 4}} \tag{69}$$

where

$$\text{Case 1} = \left\{\frac{X\beta\tau}{1-\tau} \ge \frac{Z\tau}{1-\tau}, \frac{Z\tau}{1-\tau} \le \frac{Y(1-\beta)\tau}{(Y\beta-1)\tau+1}\right\}$$

$$\text{Case 2} = \left\{\frac{X\beta\tau}{1-\tau} \ge \frac{Z\tau}{1-\tau}, \frac{Z\tau}{1-\tau} \ge \frac{Y(1-\beta)\tau}{(Y\beta-1)\tau+1}\right\}$$

$$\text{Case 3} = \left\{\frac{X\beta\tau}{1-\tau} \le \frac{Z\tau}{1-\tau}, \frac{X\beta\tau}{1-\tau} \le \frac{Y(1-\beta)\tau}{(Y\beta-1)\tau+1}\right\}$$

$$\text{Case 4} = \left\{\frac{X\beta\tau}{1-\tau} \le \frac{Z\tau}{1-\tau}, \frac{X\beta\tau}{1-\tau} \ge \frac{Y(1-\beta)\tau}{(Y\beta-1)\tau+1}\right\}$$

By comparing the optimal rates obtained from (Q1) − (Q4), we take the maximum as the max-min rate for our system. For the sake of analysis, we present the following lemma:

Lemma 4: Both $F(\tau) = (1-\tau)\ln(1+ah(\tau))$ and $G(\tau) = (1-\tau)\ln(1+\frac{(1-\beta)h(\tau)}{\beta h(\tau)+c})$ are concave functions of τ, where a, c and β are constants and $h(\tau) = \frac{\tau}{1-\tau}$.

Proof: By taking the second derivative of $F(\tau)$ and $G(\tau)$, we have

$$\frac{\partial^2 F(\tau)}{\partial\tau^2} = -\frac{a^2}{(1-\tau+a\tau)^2(1-\tau)} \tag{70}$$

$$\frac{\partial^2 G(\tau)}{\partial\tau^2} = \frac{1}{(1-\tau)^3}\left[\frac{1}{(\frac{\tau}{1-\tau}+\frac{c}{\beta})^2} - \frac{1}{(\frac{\tau}{1-\tau}+c)^2}\right] \tag{71}$$

Obviously, $\frac{\partial^2 F(\tau)}{\partial\tau^2} < 0$, $\frac{\partial^2 G(\tau)}{\partial\tau^2} < 0$. Therefore, $G(\tau)$ and $F(\tau)$ are concave function. This completes the proof. ■

For problem (Q1), after some mathematical operations, we can rewrite it as following form:

$$\max_{\tau,\beta} \frac{1-\tau}{2}\log_2\left(1+\frac{Z\tau}{1-\tau}\right) \tag{72a}$$

$$\text{s.t. } \beta \ge Z/X \tag{72b}$$

$$\beta \le \frac{(Y-Z)(1-\tau)}{YZ\tau+Y(1-\tau)} \tag{72c}$$

From (72b) and (72c), one can observe that only when $\frac{Z}{X} \le \frac{(Y-Z)(1-\tau)}{YZ\tau+Y(1-\tau)}$, the optimal solutions may be existed. In this case, we can obtain $(YZ^2+XY-XZ-YZ)\tau \le XY-XZ-YZ$, from which it can found that when $XY-XZ-YZ \le 0$, τ^* is not existed. This is due to the fact: when $XY-XZ-YZ \le 0$ and $XY-XZ-YZ+YZ^2 \le 0$, there will be $\tau > 1$. Since $0 \le \tau < 1$, τ^* is not existed; when $XY-XZ-YZ \le 0$ and $XY-XZ-YZ+YZ^2 > 0$, the inequality will not hold and thus the same conclusion can be obtained. While when $XY-XZ-YZ > 0$, the feasible domain of τ will become $\tau \le \tau_0$ with $\tau_0 = \frac{XY-XZ-YZ}{XY-XZ-YZ+YZ^2}$. Utilizing Lemma 4, we can obtain $\tau^* = \min\{\tau_Z, \tau_0\}$, where $\tau_Z = \frac{e^{W(\frac{Z-1}{e})+1}-1}{e^{W(\frac{Z-1}{e})+1}-1+Z}$ and it is the point that maximizes I_3. Note that hereafter $W(\cdot)$ denotes Lambert W function [42].

For problem (Q2), by transforming the constraints, it can be expressed as

$$\max_{\tau,\beta} \frac{1-\tau}{2}\log_2\left(1+\frac{Y(1-\beta)\tau}{Y\beta\tau+1-\tau}\right) \tag{73a}$$

$$s.t.\ \beta \ge \max\left\{\frac{Z}{X}, \frac{(Y-Z)(1-\tau)}{YZ\tau+Y(1-\tau)}\right\} \tag{73b}$$

To proceed, we first examine whether $\frac{(Y-Z)(1-\tau)}{YZ\tau+Y(1-\tau)}$ is within the effective interval of β. Let $\frac{(Y-Z)(1-\tau)}{YZ\tau+Y(1-\tau)} < 1$, we can obtain

$YZ\tau + Z(1-\tau) > 0$, so $0 < \frac{(Y-Z)(1-\tau)}{YZ\tau+Y(1-\tau)} < 1$ always holds. To obtain the optimal β and τ, we consider two cases:

- When $\frac{Z}{X} \leq \frac{(Y-Z)(1-\tau)}{YZ\tau+Y(1-\tau)}$, we have $\beta^* = \frac{(Y-Z)(1-\tau)}{YZ\tau+Y(1-\tau)}$ since the objective function is a decreasing function w.r.t. β. In this case, the constraint for $(YZ^2 + XY - XZ - YZ)\tau \leq XY - XZ - YZ$ must be satisfied for τ. Referring to (Q1), it can be found that only when $YX - ZX - YZ > 0$, the feasible domain of τ is not empty. Substituting β^* into (73), we have

$$\tau^* = \arg\max_{0<\tau\leq\tau_0} \frac{1-\tau}{2}\log_2\left(1+\frac{Z\tau}{1-\tau}\right) \tag{74}$$

  Similar to (Q1), we can obtain $\tau^* = \min\{\tau_Z, \tau_0\}$.
- When $\frac{Z}{X} \geq \frac{(Y-Z)(1-\tau)}{YZ\tau+Y(1-\tau)}$, if $\frac{Z}{X} \geq 1$, no solutions exist for (73), and if $\frac{Z}{X} < 1$, we have $\beta^* = \frac{Z}{X}$. In this case, the constraint on τ becomes $(YZ^2+XY-XZ-YZ)\tau \geq XY-XZ-YZ$.
  - when $XY-XZ-YZ \leq 0$, whether $YZ^2+XY-XZ-YZ$ is positive or negative, the feasible of τ will be $\tau \in [0, 1]$. Substituting β^* into (73), we have

$$\tau^* = \arg\max_{0\leq\tau<1} \frac{1-\tau}{2}\log_2\left(1+\frac{Y(1-Z/X)\tau}{YZ\tau/X+1-\tau}\right) \tag{75}$$

    Invoking Lemma 4, we can find that the objective function is concave w.r.t. τ and thus τ^* can be found via GSS method.
  - when $XY - XZ - YZ > 0$, we have $\tau \geq \tau_0$. Similarly, substituting β^* into (73) and based on the concave property of the objective function, we can obtain $\tau^* = \min\{\tau_0, \tau_Y\}$, where τ_Y is the solution to problem (75).

For (Q3), by doing some transformations, we have

$$\max_{\tau,\beta} \frac{1-\tau}{2}\log_2\left(1+\frac{X\beta\tau}{1-\tau}\right) \tag{76a}$$
$$\text{s.t. } 0 \leq \beta \leq Z/X \tag{76b}$$
$$F(\beta) \leq 0 \tag{76c}$$

where $F(\beta) = XY\tau\beta^2 + (X+Y)(1-\tau)\beta - Y(1-\tau)$. Since $F(\beta)$ is a quadratic function w.r.t. β, by computing its discriminant: $\Delta = [(X+Y)(1-\tau)]^2 + 4XY^2\tau(1-\tau)$, we can find $\Delta \geq 0$ and thus (76c) holds for region $\beta_L \leq \beta \leq \beta_H$, where $\beta_L = \frac{-(X+Y)(1-\tau)-\sqrt{\Delta}}{2XY\tau}$ and $\beta_H = \frac{-(X+Y)(1-\tau)+\sqrt{\Delta}}{2XY\tau}$ are the solutions of equation $F(\beta) = 0$. As $\beta_L < 0$, the feasible domain of β will become $0 \leq \beta \leq \min\{\beta_H, Z/X, 1\}$. Since the objective function in (76) is an increasing function w.r.t. β, we can obtain $\beta^* = \min\{\beta_H, Z/X, 1\}$. In order to find τ^*, two cases need to be discussed:

- When $\frac{Z}{X} \geq \beta_H$, we have $\beta^* = \beta_H$ and τ needs to satisfy $(YZ^2+XY-XZ-YZ)\tau \geq XY-XZ-YZ$. Similarly, when $XY-XZ-YZ \leq 0$, the feasible domain of τ will become $\tau \in [0, 1]$. Substituting β^* into (76), there will be

$$\tau^* = \arg\max_{0\leq\tau<1} F(\tau) \tag{77}$$

  where $F(\tau) = \frac{1-\tau}{2}\log_2(1+\frac{-(X+Y)+\Lambda}{2Y})$ with $\Lambda = \sqrt{\Delta}/(1-\tau)$. By taking derivation of $F(\tau)$, it can be shown that $\frac{\partial^2 F(\tau)}{\partial\tau^2} = -\frac{2(XY^2)^2(2Y+2\Lambda-(X+Y))}{[2Y+\Lambda-(X+Y)]^2\Lambda} \leq 0$. Therefore, $F(\tau)$ is concave w.r.t. τ and the GSS method can be exploited to find τ^*. When $XY-XZ-YZ > 0$, the feasible domain of τ will be $\tau_0 \leq \tau < 1$. In this case, τ^* that maximizes $F(\tau)$ can be found within the range of $[\tau_0, 1]$ using GSS method.
- When $\frac{Z}{X} \leq \beta_H$, we have $\beta^* = \frac{Z}{X}$ and τ needs to satisfy $(YZ^2+XY-XZ-YZ)\tau \leq XY-XZ-YZ$. Similarly, only when $XY - XZ - YZ > 0$, the feasible domain of τ is not empty. As a result, substituting β^* into (76), the optimization problem will become

$$\arg\max_{0\leq\tau\leq\tau_0} \frac{1-\tau}{2}\log_2\left(1+\frac{Z\tau}{1-\tau}\right) \tag{78}$$

  Based on the concave property of the objective function, we have $\tau^* = \min\{\tau_0, \tau_Z\}$.

The solving process of (Q4) can refer to (Q1) – (Q3), here we only list the final results: only when $\beta_H \leq \frac{Z}{X}$, the solutions may be existed. In this case, the optimal power is $\beta^* = \beta_H$. Substituting β^* into the objective function, one can observe that

- When $XY - XZ - YZ \leq 0$, the feasible domain of τ is $[0, 1]$, and τ^* that maximizes $F(\tau) = \frac{1-\tau}{2}\log_2(1+\frac{-(X+Y)+\Lambda}{2Y})$ can be found using GSS method.
- When $XY - XZ - YZ > 0$, the feasible domain of τ is $[\tau_0, 1]$. To this end, GSS method can be used to find τ^* to maximize $F(\tau)$.

By comparing the rates obtained from (Q1)-(Q4), we take the maximum one as the final max-min rate. Since the results are composed of closed-form solutions and the solutions obtained by GSS, we called it as CS-GSS method. As reported in [43], the computation complexity of GSS is $\log_2(\frac{1}{\varepsilon})$, where ε denotes the search accuracy. With the same search accuracy, the complexity of two-dimensional search will be $\frac{1}{\varepsilon^2}$. Obviously, compared with two-dimensional exhaustive search method, CS-GSS method to compute τ^* and β^* has less complexity.

V. NUMERICAL RESULTS

In this section, numerical results are provided to verify the correctness of the analyses and examine the performance of WP-CNOMA. In our considered system, the locations of S, D_1 and D_2 are $(0, 0)$, $(4, 0)$, and $(10, 0)$, respectively. Similar to [36], we assume the relay nodes have the same coordinates and locate at $(6, 0)$. Moreover, we set the path loss factor as $\alpha = 2$, the power allocation coefficients associated with NOMA as $\beta_1 = 0.15$ and $\beta_2 = 0.85$, the EH efficiency as $\eta = 0.74$ and the noise power as -20 dBm. The number of Gaussian-Chebyshev quadrature approximation terms is set as $L = 20$. The bandwidth is 1Hz. As for the target rates, we assume $R_{1,th} = 0.8$ bps/Hz and $R_{2,th} = 0.4$ bps/Hz unless otherwise specified.

For comparison, the OMA scheme is also simulated, in which the first duration of τT is used for B to charge S and R, then in the subsequent $\frac{(1-\tau)T}{2}$ duration, dividing the bandwidth equally into two parts, S utilizes one part to transmit x_1 to D_1 with energy $\beta_1 E_S$ and uses another part to transmit x_2 to R with energy $\beta_2 E_S$. Finally, R spends the remaining time to forward x_2 to D_2. On the other hand, to show the gains brought by MES and MER, the random antenna selection (RAS) is also presented. In later simulations, we use label $H-J$ to denote the combination scheme for antenna selection scheme H and multiple access technique J, where $H \in \{\text{MES, MER, RAS}\}$ and $J \in \{\text{NOMA, OMA}\}$.

A. THE PERFORMANCE OF WP-CNOMA UNDER LINEAR EH SCHEME

In Fig. 3, we investigate the performance of MES and MER versus the position of PB with different antenna-relay pairings (N,K), where $\tau = 0.4$ and $\beta_1 = 0.15$. Since MES, MER and RAS are be equivalent to each other when $N = 1$ and $K = 1$, the OPs of MES and MER in such case are omitted here. From the figure, one can observe that for D_1, its OP decreases with PB moving towards S since S can harvest more energy in this case. Moreover, as N increases, the OP of D_1 for MES decreases significantly, while MER and RAS stay the same. Therefore, from the prospective of the OP of D_1, MES outperforms MER and RAS. As for D_2, we can find that when $N = 1$ and $K = 1$, the optimal position of PB is at the point closer to S, which may be due to $d_{SR} < d_{S2}$. With the increase of N, the optimal position of PB for MES begins to move towards R while that for MER continues moving towards S. This can be explained by the fact that the performance of D_2 is jointly determined by the $S-R$ link and $R-D_2$ link, and MES only considers to maximize the harvested energy of S. To minimize the OP of D_2, it's reasonable to improve the quality of cooperative link by moving PB towards R. Similarly, MER only considers to select the antenna that maximizes the harvested energy of R, i.e., the reception of $R-D_2$ link is improved. To minimize the OP of D_2, PB should move towards S to improve the quality of $S-R$ link. In addition, relay selection can also be used to improve the channel of cooperative link. Specifically, when the number of candidate relays increases, the optimal positions of PB for MES and MER schemes begin to move towards S. From the above observations, we can find that with the aid of relay selection, the cooperative link can be improved significantly. By combining antenna selection and relay selection, the OPs of D_1 and D_2 can be decreased greatly. By weighing the outage behaviors of D_1 and D_2 described above, in what follows, we set the position of PB at (2,2).

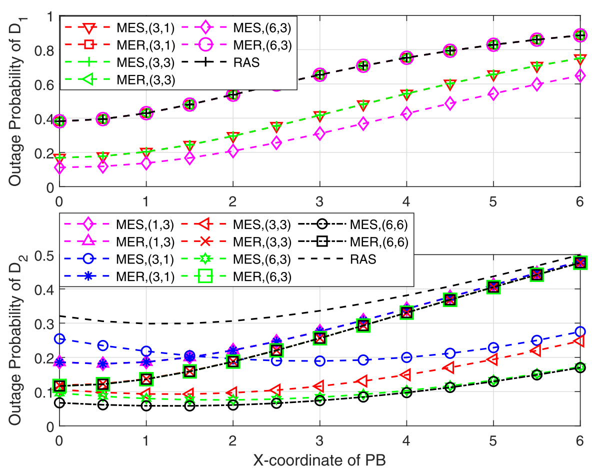

FIGURE 3. The effect of the location of PB on the OPs of D_1 and D_2, where the y-coordinate of PB is 2.

Fig. 4 illustrates the effects of EH time and power allocation on the performance of WP-CNOMA system, where $N = 3$, $K = 3$ and $P_B = 20$ dBm. As shown in the figure, when τ is bigger than a certain value, the average throughput will be 0, which results from the fact that the OPs of D_1 and D_2 will be 1 when $\omega_2 > \beta_2/\beta_1$. In addition, we can find that for a wide range of EH time from 0 to a certain value, whether for MES or for MER, NOMA scheme has better performance than the OMA scheme due to higher spectral efficiency.

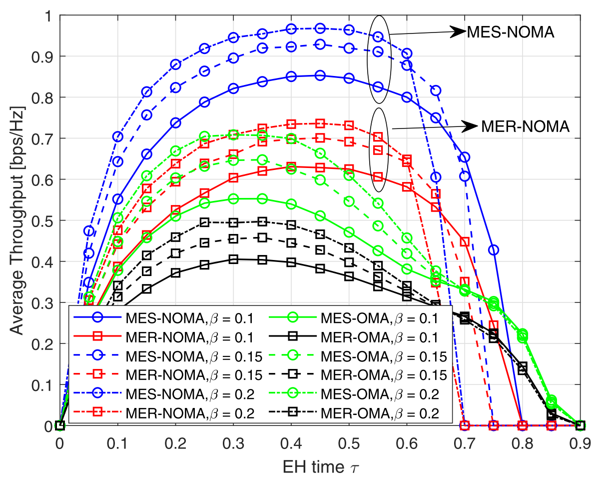

FIGURE 4. The effects of EH time and power allocation on the performance of WP-CNOMA system.

Fig. 5 shows the simulated and analytical OPs of D_1 and D_2, where $N = 3$, $K = 3$, $\tau = 0.4$ and $\beta_1 = 0.15$. One can see that the simulated results match well with the analytical ones, which verifies the correctness of our analyses. Moreover, whether for D_1 or for D_2, compared with OMA, NOMA schemes achieve more superior outage performance as expected. In addition, one can see that for D_1, the performance for MES is better than that of MER/RAS, and MER and RAS are identical to each other; while for D_2, MES is best, second is MER and RAS is the worst. As explained in Fig. 3, by applying antenna-relay selection, MES improves the reception of direct link by selecting the antenna that maximizes the transmit power of S and improves the quality of cooperative link by selecting the best relay towards D_2.

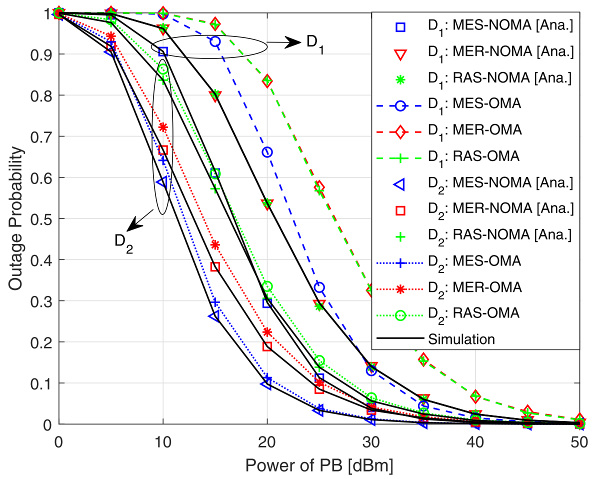

FIGURE 5. The simulated and analytical OPs of D_1 and D_2.

Whereas MER only improves the quality of cooperative link, its performance is constrained by the quality of direct link.

In Fig. 6, we investigate the effects of both antenna number and relay number on the OPs of D_1 and D_2. First, as shown in Fig. 6(a), the OP of D_1 in MER will not change with the number of antennas, while that in MES will decrease with the number of antennas and the OPs of D_2 in both schemes decrease with N. These phenomena can be explained by the fact that in MES, benefitting from the antenna diversity, S can harvest more energy from PB, and combined with relay selection, the performance of both D_1 and D_2 can be improved; in MER, the increase of N only contributes to the performance improvement for $R-D_2$ link, and has no effect on the performance of D_1. With respect to the effect of K, it can be seen from Fig. 6(b) that only D_2 is affected by K and its OP decreases with the increase of K whether for MES or for MER, since better $R-D_2$ link can be provided in this case. In addition, it should be noted that comparing with MES, the performance improvement for MER is limited with the increase of N or K, which is caused by the fact that MER only improves the quality of $R-D_2$ link and thus its performance is restricted by the quality of $S-R$ link.

B. PERFORMANCE COMPARISON OF WP-CNOMA SYSTEM WITH LINEAR EH AND NON-LINEAR EH

In this subsection, we compare the outage performance of WP-CNOMA system for linear EH and non-linear EH models. Here two cases of saturated power modeling for non-linear EH scheme are considered. For Case 1 (C1), in line with [35], we assume P^s_{th} and P^r_{th} are proportional to the transmit power of PB. While for Case 2 (C2), we assume both P^s_{th} and P^r_{th} are constants [38]. For simplicity, we assume $P^s_{th} = P^r_{th} = P_{th}$ and thus the superscripts for s and r will be omitted in later figures. In addition, we use 'nMES-NOMA' and 'nMER-NOMA' to denote the non-linear EH WP-CNOMA system based on MES and MER, respectively.

In Fig. 7, we compare the outage performance for WP-CNOMA with linear EH and non-linear EH, where for C1, we assume $P_{th}/P_B = -5$ dB and for C2, we assume $P_{th} = 20$ dBm. Note that the performance gain for MES/MER over RAS has been confirmed in the previous part, so RAS scheme is not considered in this figure. As can be seen, the analytical results match well with the simulated ones, which validates the correctness for our analyses associated with the non-linear EH schemes. In addition, we observe that the OPs under C1 are almost similar to those under linear EH, while the OPs under C2 are perfectly agreement with those under linear EH in low SNR region and when SNR is bigger than a certain value, the outage floors will appear and converge to constants as expected. To better explain these phenomena, in Fig. 8, we explore the outage performance for C1 and C2 with different saturated power values, where for schemes under C1, we assume $P_{th}/P_B = -15$ dB and -5 dB and for schemes under C2, we assume $P_{th} = 20$ dBm and 25 dBm. As can be observed, under C1, the OPs of D_1

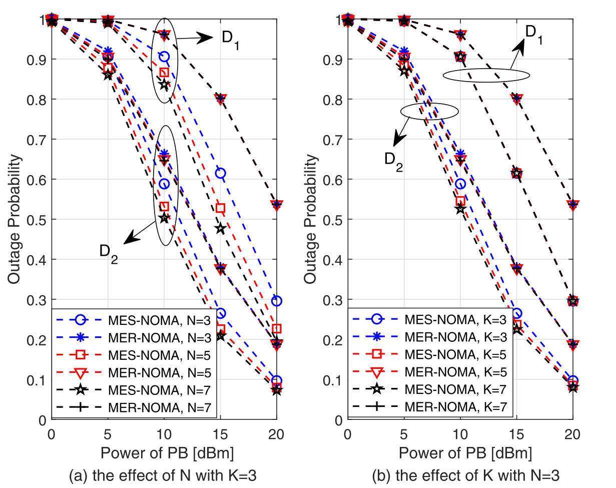

FIGURE 6. The effects of relay number and antenna number on the OPs of D_1 and D_2.

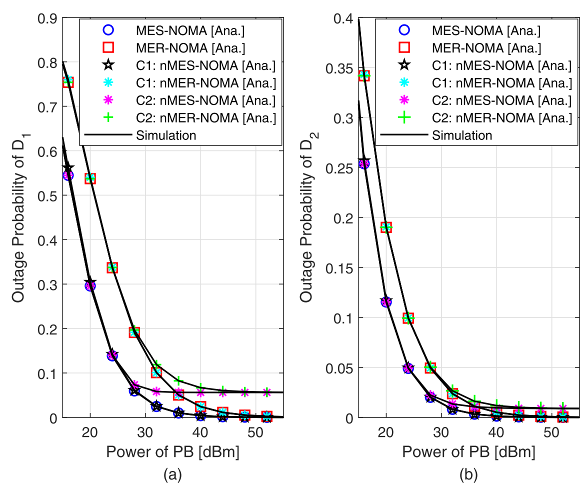

FIGURE 7. The OP comparisons of linear EH and non-linear EH.

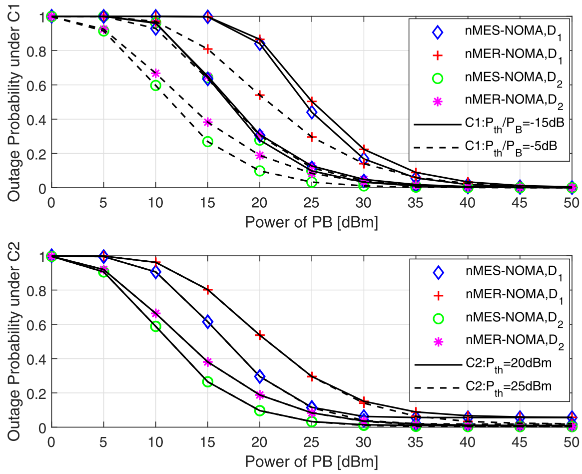

FIGURE 8. The effect of values for saturated power on the OPs for non-linear EH WP-CNOMA system.

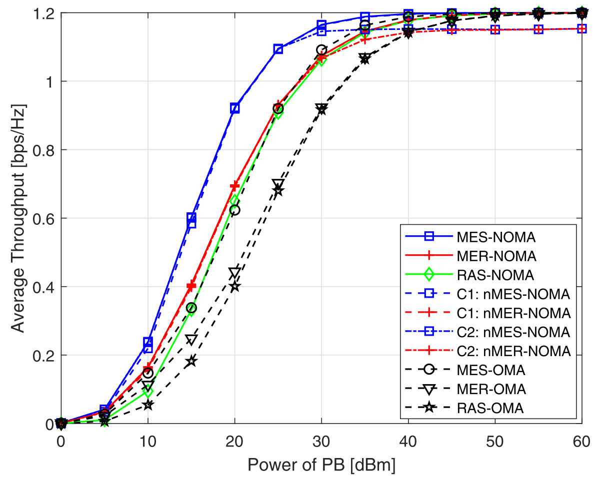

FIGURE 9. The average throughput for WP-CNOMA system.

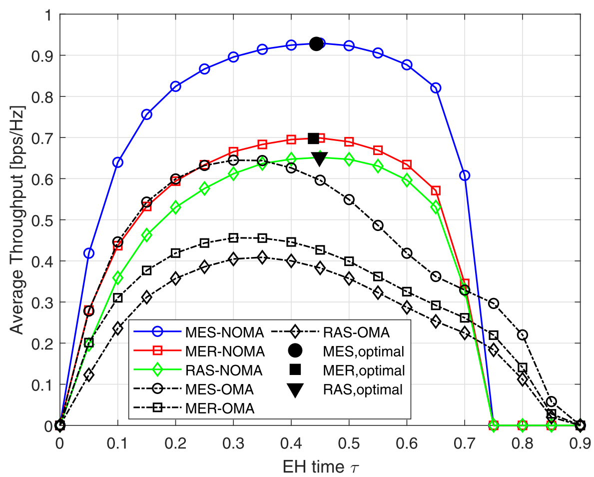

FIGURE 10. The average throughput versus the EH time.

and D_2 are greatly affected by the setting of the saturated threshold, specially, 1) when P_{th}/P_B is fixed, the OPs of D_1 and D_2 decrease with the increase of P_B, which results from the fact that according to (10)-(13), when P_{th}/P_B is given, the working state is also determined. In this case, OP can be improved with the increase of P_B. 2) when P_B is fixed, the OPs of D_1 and D_2 will also decrease with the increase of P_{th}/P_B. This can be well understood since with fixed P_B, the increase of P_{th}/P_B means the increase of P_{th}. In this case, it's likely that system will work in linear EH state and more energy can be harvested, and thus the outage performance can be improved. While under C2, we can see that when P_{th} is large enough, only the performance in high SNR region is significantly affected by P_{th}. With fixed P_B, the outage floor will decrease with the increase of P_{th}. Moreover, the larger P_{th}, the later the outage floor appears. Both of results are due to the fact that more energy can be harvested with the increase of P_{th}.

Fig. 9 investigates the average throughput performance for WP-CNOMA system. It can be observed that among these schemes, the MES-NOMA schemes have the largest throughput, followed by MER-NOMA and then RAS-NOMA. Moreover, all the NOMA schemes show superior performance than the OMA schemes as expected. Compared with linear EH schemes, the non-linear EH schemes under C1 show slightly worse throughput in low-medium SNR region, but in high SNR region, since the outage will not occur, both linear and non-linear EH schemes will own the same throughput. While the non-linear EH schemes under C2 keep the pace with linear EH schemes in low-medium SNR region, and they will converge to constants in high SNR region due to the constant saturated threshold in C2.

Fig. 10 shows the average system throughput with respect to EH time, where $P_B = 20$ dBm. As can be seen from the figure, the average throughput of each scheme is an unimodal function of EH time, in which it first increases when τ varies from 0 to the optimal τ and then begins to decrease when τ continues to increase. This can be well understood since with smaller τ, the harvest energy will be small; with the increase of τ, more energy can be harvested so that throughput will increase; with larger τ, less time is allocated for WIT and thus throughput is small. Invoking the unimodal property, we use the Golden section search method to find the optimal EH time for these NOMA schemes, which have been marked in Fig. 10.

C. PERFORMANCE OPTIMIZATION

Fig. 11 shows the max-min rate achieved by our system with $N = 1$ and $K = 1$, and the linear EH scheme is considered. Here OTOP denotes the case that the EH time and power allocation are jointly optimized, OTFP denotes the case that the EH time is optimized with fixed power allocation, FTOP denotes the power allocation is optimized with fixed EH time and FTFP denotes the case in which both time and power are fixed. As shown in the figure, the analytical results are in accordance with those obtained by two-dimensional search, which verifies the correctness of the optimization analyses.

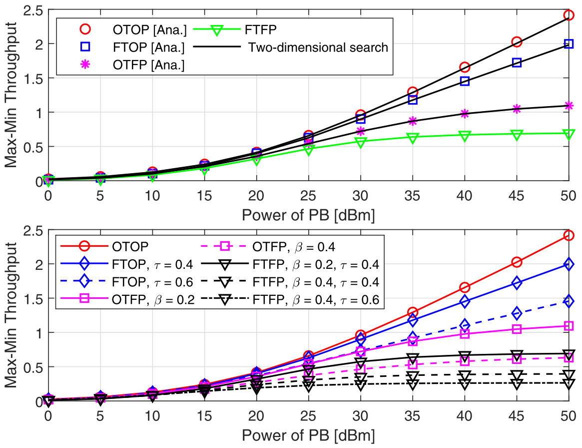

FIGURE 11. The max-min throughput versus the power of PB.

Moreover, as expected, OTOP scheme outperforms the other three schemes and FTFP has the worst performance. In addition, it can be observed that for OTOP, FTOP and OTFP schemes, their max-min throughput increase with the power of PB and compared with OTOP and FTOP, the throughput growth of FTFP and OTFP will tend to be slow in high SNR region. These phenomena reflect the necessity for joint optimization of power allocation and EH time to improve the performance for WP-CNOMA system.

VI. CONCLUSION

In this paper, we propose a downlink WP-CNOMA system, in which PB is introduced to charge energy-constraint S and R. To effectively improve the system performance, low-complexity antenna selection and relay selection are applied. For such a system, we first derive the closed-form outage probabilities of two receivers and the average throughput considering the linear EH model. While those under non-linear EH model are presented as well. By simulation, it has been shown that the theoretical analyses are in good agreement with the simulated results and the superiority of WP-CNOMA system over the corresponding OMA one has also been validated with proper power allocation and EH time. In addition, it has been found that the outage performance in non-linear EH model shows different behavior with the linear one. Also, invoking the unimodal property for average throughput on EH time, we exploit the Golden section search method to find the optimal EH time. On the other hand, assuming perfect CSI is known, a minimum achievable rate maximization optimization is developed to jointly optimize the EH time and power allocation and the max-min rate is obtained semi-analytically. Compared with two-dimensional search, our method has lower computation complexity and requires less computation time. Simulation results show that the system performance can be significantly improved by jointly optimizing time and power. In the future work, we will further consider the analysis for the case where beamforming-based WPT is applied and the practical problem of imperfect SIC will also be considered.

REFERENCES

[1] N. Zhao, W. Lu, M. Sheng, Y. Chen, J. Tang, F. R. Yu, and K.-K. Wong, "UAV-assisted emergency networks in disasters," *IEEE Wireless Commun.*, vol. 26, no. 1, pp. 45–51, Feb. 2019.

[2] R. Zhang and C. K. Ho, "MIMO broadcasting for simultaneous wireless information and power transfer," *IEEE Trans. Wireless Commun.*, vol. 12, no. 5, pp. 1989–2001, May 2013.

[3] K. Huang and V. K. N. Lau, "Enabling wireless power transfer in cellular networks: Architecture, modeling and deployment," *IEEE Trans. Wireless Commun.*, vol. 13, no. 2, pp. 902–912, Feb. 2014.

[4] L. Liu, R. Zhang, and K.-C. Chua, "Wireless information transfer with opportunistic energy harvesting," *IEEE Trans. Wireless Commun.*, vol. 12, no. 1, pp. 288–300, Jan. 2013.

[5] L. Liu, R. Zhang, and K.-C. Chua, "Wireless information and power transfer: A dynamic power splitting approach," *IEEE Trans. Commun.*, vol. 61, no. 9, pp. 3990–4001, Sep. 2013.

[6] W. Chen, H. Ding, S. Wang, D. B. da Costa, and F. Gong, "Impartial SWIPT-assisted user cooperation schemes," *IEEE Trans. Wireless Commun.*, vol. 19, no. 5, pp. 3361–3375, May 2020.

[7] J. Ye, Z. Liu, H. Zhao, G. Pan, Q. Ni, and M.-S. Alouini, "Relay selections for cooperative underlay CR systems with energy harvesting," *IEEE Trans. Cognit. Commun. Netw.*, vol. 5, no. 2, pp. 358–369, Jun. 2019.

[8] Y. Huang, M. Liu, and Y. Liu, "Energy-efficient SWIPT in IoT distributed antenna systems," *IEEE Internet Things J.*, vol. 5, no. 4, pp. 2646–2656, Aug. 2018.

[9] N.-P. Nguyen, T. Q. Duong, H. Q. Ngo, Z. Hadzi-Velkov, and L. Shu, "Secure 5G wireless communications: A joint relay selection and wireless power transfer approach," *IEEE Access*, vol. 4, pp. 3349–3359, 2016.

[10] C. Zhong, H. Liang, H. Lin, H. A. Suraweera, F. Qu, and Z. Zhang, "Energy beamformer and time split design for wireless powered two-way relaying systems," *IEEE Trans. Wireless Commun.*, vol. 17, no. 6, pp. 3723–3736, Jun. 2018.

[11] Y. Liu, S. A. Mousavifar, Y. Deng, C. Leung, and M. Elkashlan, "Wireless energy harvesting in a cognitive relay network," *IEEE Trans. Wireless Commun.*, vol. 15, no. 4, pp. 2498–2508, Apr. 2016.

[12] C. Zhai, H. Chen, Z. Yu, and J. Liu, "Cognitive relaying with wireless powered primary user," *IEEE Trans. Commun.*, vol. 67, no. 3, pp. 1872–1884, Mar. 2019.

[13] S. Yin, L. Li, and F. R. Yu, "Resource allocation and basestation placement in downlink cellular networks assisted by multiple wireless powered UAVs," *IEEE Trans. Veh. Technol.*, vol. 69, no. 2, pp. 2171–2184, Feb. 2020.

[14] L. Xie, J. Xu, and R. Zhang, "Throughput maximization for UAV-enabled wireless powered communication networks," *IEEE Internet Things J.*, vol. 6, no. 2, pp. 1690–1703, Apr. 2019.

[15] Y. Saito, Y. Kishiyama, A. Benjebbour, T. Nakamura, A. Li, and K. Higuchi, "Non-orthogonal multiple access (NOMA) for cellular future radio access," in *Proc. IEEE 77th Veh. Technol. Conf. (VTC Spring)*, Jun. 2013, pp. 1–5.

[16] Z. Ding, P. Fan, and H. V. Poor, "Impact of user pairing on 5G nonorthogonal multiple-access downlink transmissions," *IEEE Trans. Veh. Technol.*, vol. 65, no. 8, pp. 6010–6023, Aug. 2016.

[17] Z. Ding, M. Peng, and H. V. Poor, "Cooperative non-orthogonal multiple access in 5G systems," *IEEE Commun. Lett.*, vol. 19, no. 8, pp. 1462–1465, Aug. 2015.

[18] Z. Zhang, Z. Ma, M. Xiao, Z. Ding, and P. Fan, "Full-duplex device-to-device-Aided cooperative nonorthogonal multiple access," *IEEE Trans. Veh. Technol.*, vol. 66, no. 5, pp. 4467–4471, May 2017.

[19] J.-B. Kim and I.-H. Lee, "Non-orthogonal multiple access in coordinated direct and relay transmission," *IEEE Commun. Lett.*, vol. 19, no. 11, pp. 2037–2040, Nov. 2015.

[20] J. Men, J. Ge, and C. Zhang, "Performance analysis of nonorthogonal multiple access for relaying networks over nakagami-*m* fading channels," *IEEE Trans. Veh. Technol.*, vol. 66, no. 2, pp. 1200–1208, Feb. 2017.

[21] P. Xu, Z. Yang, Z. Ding, and Z. Zhang, "Optimal relay selection schemes for cooperative NOMA," *IEEE Trans. Veh. Technol.*, vol. 67, no. 8, pp. 7851–7855, Aug. 2018.

[22] L. Zhang, J. Liu, M. Xiao, G. Wu, Y.-C. Liang, and S. Li, "Performance analysis and optimization in downlink NOMA systems with cooperative full-duplex relaying," *IEEE J. Sel. Areas Commun.*, vol. 35, no. 10, pp. 2398–2412, Oct. 2017.

[23] X. Chen, G. Liu, Z. Ma, X. Zhang, W. Xu, and P. Fan, ''Optimal power allocations for non-orthogonal multiple access over 5G full/half-duplex relaying mobile wireless networks,'' *IEEE Trans. Wireless Commun.*, vol. 18, no. 1, pp. 77–92, Jan. 2019.
[24] J. Tang, J. Luo, M. Liu, D. K. C. So, E. Alsusa, G. Chen, K.-K. Wong, and J. A. Chambers, ''Energy efficiency optimization for NOMA with SWIPT,'' *IEEE J. Sel. Topics Signal Process.*, vol. 13, no. 3, pp. 452–466, Jun. 2019.
[25] J. Tang, Y. Yu, M. Liu, D. K. C. So, X. Zhang, Z. Li, and K.-K. Wong, ''Joint power allocation and splitting control for SWIPT-enabled NOMA systems,'' *IEEE Trans. Wireless Commun.*, vol. 19, no. 1, pp. 120–133, Jan. 2020.
[26] Y. Liu, Z. Ding, M. Elkashlan, and H. V. Poor, ''Cooperative non-orthogonal multiple access with simultaneous wireless information and power transfer,'' *IEEE J. Sel. Areas Commun.*, vol. 34, no. 4, pp. 938–953, Apr. 2016.
[27] T. N. Do, D. B. da Costa, T. Q. Duong, and B. An, ''Improving the performance of cell-edge users in MISO-NOMA systems using TAS and SWIPT-based cooperative transmissions,'' *IEEE Trans. Green Commun. Netw.*, vol. 2, no. 1, pp. 49–62, Mar. 2018.
[28] Y. Zhang, J. Ge, and E. Serpedin, ''Performance analysis of a 5G energy-constrained downlink relaying network with non-orthogonal multiple access,'' *IEEE Trans. Wireless Commun.*, vol. 16, no. 12, pp. 8333–8346, Dec. 2017.
[29] G. Li, D. Mishra, Y. Hu, and S. Atapattu, ''Optimal designs for relay-assisted NOMA networks with hybrid SWIPT scheme,'' *IEEE Trans. Commun.*, vol. 68, no. 6, pp. 3588–3601, Jun. 2020.
[30] Y. Xu, C. Shen, Z. Ding, X. Sun, S. Yan, G. Zhu, and Z. Zhong, ''Joint beamforming and power-splitting control in downlink cooperative SWIPT NOMA systems,'' *IEEE Trans. Signal Process.*, vol. 65, no. 18, pp. 4874–4886, Sep. 2017.
[31] P. D. Diamantoulakis, K. N. Pappi, Z. Ding, and G. K. Karagiannidis, ''Wireless-powered communications with non-orthogonal multiple access,'' *IEEE Trans. Wireless Commun.*, vol. 15, no. 12, pp. 8422–8436, Dec. 2016.
[32] Z. Chen, K. Chi, K. Zheng, Y. Li, and X. Liu, ''Common throughput maximization in wireless powered communication networks with non-orthogonal multiple access,'' *IEEE Trans. Veh. Technol.*, vol. 69, no. 7, pp. 7692–7706, Jul. 2020.
[33] Q. Wu, W. Chen, D. W. K. Ng, and R. Schober, ''Spectral and energy-efficient wireless powered IoT networks: NOMA or TDMA?'' *IEEE Trans. Veh. Technol.*, vol. 67, no. 7, pp. 6663–6667, Jul. 2018.
[34] P. Deng, B. Wang, W. Wu, and T. Guo, ''Transmitter design in MISO-NOMA system with wireless-power supply,'' *IEEE Commun. Lett.*, vol. 22, no. 4, pp. 844–847, Apr. 2018.
[35] J. Zhang, G. Pan, and Y. Xie, ''Secrecy analysis of wireless-powered multi-antenna relaying system with nonlinear energy harvesters and imperfect CSI,'' *IEEE Trans. Green Commun. Netw.*, vol. 2, no. 2, pp. 460–470, Jun. 2018.
[36] H. Chen, Y. Li, J. Luiz Rebelatto, B. F. Uchoa-Filho, and B. Vucetic, ''Harvest-Then-cooperate: Wireless-powered cooperative communications,'' *IEEE Trans. Signal Process.*, vol. 63, no. 7, pp. 1700–1711, Apr. 2015.
[37] E. Boshkovska, D. W. K. Ng, L. Dai, and R. Schober, ''Power-efficient and secure WPCNs with hardware impairments and non-linear EH circuit,'' *IEEE Trans. Commun.*, vol. 66, no. 6, pp. 2642–2657, Jun. 2018.
[38] X. Xie, J. Chen, and Y. Fu, ''Outage performance and QoS optimization in full-duplex system with non-linear energy harvesting model,'' *IEEE Access*, vol. 6, pp. 44281–44290, 2018.
[39] Q. Wu and R. Zhang, ''Common throughput maximization in UAV-enabled OFDMA systems with delay consideration,'' *IEEE Trans. Commun.*, vol. 66, no. 12, pp. 6614–6627, Dec. 2018.
[40] I. S. Gradshteyn and I. M. Ryzhik, *Table of Integrals, Series, and Products*, 7th ed. New York, NY, USA: Academic, 2007.
[41] L. Kiefer, ''Sequential minimax search for a maximum,'' *Proc. Amer. Math. Soc.*, vol. 4, no. 3, pp. 502–506, Jun. 1953.
[42] M. Ju and H.-C. Yang, ''Optimum design of energy harvesting relay for two-way Decode-and-Forward relay networks under Max–Min and max-sum criterions,'' *IEEE Trans. Commun.*, vol. 67, no. 10, pp. 6682–6697, Oct. 2019.
[43] S. Gong, S. Ma, C. Xing, and G. Yang, ''Optimal beamforming and time allocation for partially wireless powered sensor networks with downlink SWIPT,'' *IEEE Trans. Signal Process.*, vol. 67, no. 12, pp. 3197–3212, Jun. 2019.

YAFANG ZHANG (Student Member, IEEE) received the B.S. degree from the Inner Mongolia University of Science and Technology, Baotou, China, in 2014. She is currently pursuing the Ph.D. degree with the School of Electronic and Information Engineering, South China University of Technology, Guangzhou, China. Her research interests include cooperative communications, energy harvesting, and non-orthogonal multiple access.

SUILI FENG (Member, IEEE) received the B.S. degree in electrical engineering from the South China Institute of Technology, Guangzhou, China, in 1982, and the M.S. and Ph.D. degrees in electronic and communication system from the South China University of Technology, Guangzhou, in 1989 and 1998, respectively. From 1991 to 1992, he was a Research Assistant with The Hong Kong Polytechnic University, Hong Kong. From 1998 to 1999, he was a Visiting Scholar with the University of South Florida, Tampa, FL, USA. Since 1989, he has been with the South China University of Technology, where he currently works as a Professor with the School of Electronic and Information Engineering. His research interests include wireless networks, computer networks, and communication signal processing.

WEIJUN TANG (Graduate Student Member, IEEE) received the B.E. degree in information engineering, and the Ph.D. degree in information and communication engineering from the South China University of Technology, Guangzhou, China, in 2012 and 2018, respectively. He is currently a Postdoctoral Fellow with the School of Electronic and Information Engineering, South China University of Technology. His research interests include future cellular networks, full duplex, low latency and ultra-reliable communications, the IoT, stochastic geometry, and resource allocation in wireless networks.